Journal of Applied Fluid Mechanics, Vol. 16, No. 5, pp. 960-972, 2023.
Available online at www.jafmonline.net, ISSN 1735-3572, EISSN 1735-3645.
https://doi.org/10.47176/jafm.16.05.1578

Measuring the Taylor Bubble Length in a Two-Phase Flow using an Electrical Resistance Sensor and a High-Speed Camera

M. H. Ramezani, R. Maddahian†, M. M. Noroozi and M. R. Ansari

Faculty of Mechanical Engineering, Tarbiat Modares University, Tehran, Iran

†*Corresponding Author Email: maddahian@modares.ac.ir*

(Received September 20, 2022; accepted January 2, 2023)

ABSTRACT

The present research aims to investigate the two-phase air/water flow in a vertical pipe using an electrical resistance sensor and a high-speed camera. An electrical resistance sensor is designed and embedded in the inner wall of the tube. A flow pattern map is drawn at the height of 270 cm from the testbed inlet for 320 different phase velocities using a high-speed camera. By measuring the output voltage of the electrical resistance sensor and using the Maxwell relation, the volume fraction in bubbly and slug flow regimes are calculated for different phase velocities. The volume fraction values detected from the output signal of the electrical resistance sensor are compared with the results obtained from the high-speed camera images. The width of the output signal from the electrical resistance sensor indicates the length of the Taylor bubble. The output signal width is compared to the obtained Taylor bubble length from high-speed camera images, for several different velocities of the phases. It is noticed that at a constant velocity of the phases, the output signal width from the sensor is linearly related to the length of the Taylor bubble. The variations of the output signal width are plotted in terms of the ratio of the Taylor bubble length to the summation of air and water superficial velocities. By linear fitting of the available data, a novel equation is presented to calculate the Taylor bubble length in terms of the signal output from the electrical resistance sensor and the total superficial velocity of the phases.

Keywords: Multiphase flow; Transient flow regime; Vertical tube; Electrical resistance tomography; Taylor bubble length; Electrical resistance sensor.

NOMENCLATURE

a	air phase	v	electric potential difference
g	gas phase	V	superficial velocity
l	liquid phase	w	water
m	two-phase	α	volume fraction
T	Taylor bubble	σ	conductivity

1. INTRODUCTION

The Gas-liquid two-phase flows are found in various industrial systems, like oil separators, distillation towers, boilers, refrigerators, air conditioners, reactors, and oil pipelines. Different parameters such as pressure drop and heat transfer coefficient depend on the flow pattern. So identifying the flow pattern and calculating the volume fraction play an effective role in operational safety, process control, and reliability of various processes (Brennen 2005). Over the past few decades, due to the important applications of two-phase flows in industry, extensive experimental and practical investigations have been conducted to examine the two-phase flows. Among several characteristics of the two-phase flow, measuring the flow volume fraction and identifying the flow regime are still the subject of new researches. In addition, regime transition is a novel and important phenomenon in multiphase flows, on which numerous numerical and experimental researches have been conducted (Kaichiro and Ishii 1984; Ishii and De Jarlais 1986; Shaikh and Al-Dahhan 2007; Höhne and Vallée 2010; Hänsch *et al*. 2012; Montoya *et al*. 2014; Kuidjo and Vianney 2019; Noroozi *et al*. 2021; Ramezani *et al*. 2021). Volume fraction measurement methods are one of the necessary tools

to better understand the regime transition phenomenon.

Volumetric fraction measurement techniques are categorized into intrusive and non-intrusive types. In intrusive techniques, the physical flow may be disturbed by the measurement probe which has direct contact with the fluids. But in non-intrusive techniques, the measurement signals are captured by the sensors mounted out of the flow (Wang *et al.* 2009). Intrusive measurement probes exist in different sorts including capacitance probe (Geldart and Kelsey 1972; Shi *et al.* 1991; Sharma *et al.* 2000), optical fiber probe (Yasui and Johanson 1958; Bayle *et al.* 2001; Cui and Chaouki 2004), endoscopic probe (Peters *et al.* 1983), and pressure transducer probe (Lirag and Littman 1971; Fan *et al.* 1981; Sitnai 1982). The intrusive measurement systems are mostly used in fluidized beds. Non-intrusive measurement techniques are used in multiphase flow systems that are sensitive to the disturbance of the internal flow. Up to now, many non-intrusive multiphase flow measurement techniques are developed including X-ray (Gilbertson *et al.* 1998; Hulme and Kantzas 2004; Hubers *et al.* 2005), gamma-ray tomography (GRT) (Wu *et al.* 2007; Patel *et al.* 2008; Schubert *et al.* 2008), positron emission tomography (PET) (Dechsiri *et al.* 2005), radioactive particle tracking (RPT) (Larachi *et al.* 1997; Larachi and Chaouki 2000), magnetic resonance imaging (MRI) (Fennell *et al.* 2005; Holland *et al.* 2009), electrical resistance tomography (ERT) (Bennett and Williams 2004; Vilar *et al.* 2008; Rasteiro *et al.* 2011), electrical capacitance tomography (ECT) (Halow and Nicoletti 1992; Du *et al.* 2004; Marashdeh *et al.* 2008; Wang *et al.* 2010) and electrical magnetic tomography (EMT) (Binns *et al.* 2001).

The purpose of the electrical resistance tomography system is to reconstruct the distribution of electrical conductivity and phases within the tube. Electrical resistance sensors typically consist of several electrodes located inside a tube in contact with a two-phase flow. The electrical voltage is measured by electrodes and the measured voltage value is related to the phase distribution (Kotze *et al.* 2019). These sensors are corroded over time due to the direct contact of the electrodes with the flow. This phenomenon reduces the measurement accuracy and thus increases costs due to the replacement of old electrodes with new ones (Tan and Dong 2010). Electrical resistance tomography is one of the most popular methods among other tomography methods due to its high data rate, low manufacturing cost, high safety, and compatibility with large and small diameter tubes (Jin *et al.* 2007).

Das and Pattanayak (1993) reported a technique to recognize the flow regime transitions in an upward vertical gas-liquid two-phase flow system using an Indigenous electronic circuit. In this method, the two-phase mixture's volume fraction signal is converted to a series of square pulses with different widths. To detect the bubble-to-slug flow transition, the probability density function of the pulse width spectra was investigated. And also the transition of the Slug flow to the churn flow regime was observed on the basis of liquid slug length measurements. Meng *et al.* (2010) proposed a measurement technique for air–water two-phase flow using a combination of an ERT sensor and a venturi meter. At first, the ERT sensor recognized the real-time flow pattern of the two-phase flow. Then, the volume fraction was determined using the conductance values through the presented volume fraction measurement method, and with the help of the void fraction-quality correlation, the mass quality was calculated from the volume fraction. Finally, the mass flow rate of the two-phase flow was determined through the mass quality and the differential pressure between the venturi meters. Zhang and Chen (2012) introduced a novel algorithm to identify the different flow patterns. The presented algorithm is working based on principal component analysis–support vector machine, principal component analysis general regression neural network, and electrical resistance system measurement. Xu *et al.* (2009) used the ERT method to distinguish the slug flow in horizontal pipes. Tan and Dong (2010) conducted several experimental investigations on gas–water two-phase flows in a horizontal pipe utilizing a V-cone meter and the ERT system. Yang *et al.* (2012) presented a dual-plane ERT method that provides a real-time measurement of air volume fraction distribution inside its sensing area. The developed system is able to make flow velocity maps and cross-sectional images. Pedersen *et al.* (2015) conducted experimental studies and proposed an ERT transmitter for online slug detection. A novel multi-electrode contactless resistivity array sensor was developed by Wahab *et al.* (2018). The developed system utilized the capacitively coupled contactless conductivity detection technique to take the measurements of the resistance of conductive gas-liquid flow. The sensor's electrodes are placed in a way to have no contact with the fluids. So it can overcome the disadvantages of conventional electrical resistance measurement sensors. Xu *et al.* (2020) introduced a novel method to carry out volume fraction measurement of gas–liquid two-phase flow. They conducted several experiments on the volume fraction measurement system by the 12-electrode contactless resistivity array sensor. According to their findings, the volume fraction measurement performances are not the same under the various excitation patterns. Five different excitation patterns were evaluated, and the pattern with five electrodes shows the best performance. Wang *et al.* (2006) used ERT to investigate the air volume fraction and the velocity distribution of gas–liquid flow in a swirling two-phase system. Jia *et al.* (2017) studied the oil-water two-phase flow with several volume fractions using ERT method and demonstrated that visualizations on both directions are available. They also experimentally validated the measurement of high conductive oil using ERT. Rehman *et al.* (2019) compared the actual images of the flow conditions using the horizontal flow loop system with real-time tomographic images of multiphase flow from ERT.

The review of the previous literature shows the

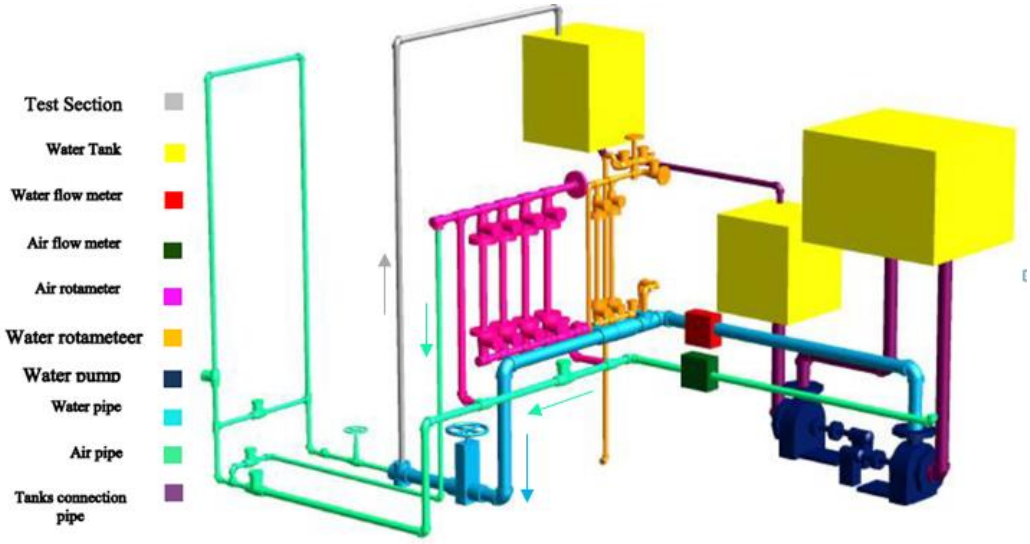

Fig. 1. Experimental system and testbed's schematic view.

efficiency of the electrical resistance sensor as a non-invasive method in the measurement of two-phase flow. From the past decades until today, by developing electrical resistance sensors, researchers have obtained important parameters such as void fraction and two-phase flow velocity using electrical resistance sensors. However, the measurement vacuum of geometrical parameters such as bubble diameter and Taylor bubble length is still felt in these sensors. Creating a method to measure flow geometric parameters using these sensors can help increase the efficiency of these sensors in the industry.

In the present work, the volume fraction is calculated by measuring the output voltage of the electrical resistance sensor. The results obtained from the electrical resistance sensor is compared with the output of the high-speed camera. By identifying the relationship between Taylor bubble length and signal width obtained from the electrical resistance sensor, a novel equation is presented to calculate the Taylor bubble length. Calculating Taylor bubble length in situations where it is not possible to observe the flow directly is useful in the various industrial systems.

2. TESTBED AND EXPERIMENTAL SYSTEM

The Experimental system used in this study is shown in Fig 1. The air and the water enter the testbed through 0.5 and 2 inch diameter pipes, respectively. The pipes are made of transparent Plexiglas. The inner diameter of the testbed tube is 50 mm, and its height is 390 cm. To generate various flow patterns, a multi-stage air diffuser is installed at the air inlet. This diffuser helps to produce uniform and homogeneous bubbles. After leaving the testbed, the air and water two-phase flow enters the tank to separate the phases from each other. An atmospheric separation tank is used to separate air and water. The collected water at the bottom of the separation tank is transferred to the water storage tank.

Fig. 2. Experimental unit and the air bubble diffuser.

An image of the experimental system built in the multiphase flow laboratory of Tarbiat Modares University is shown in Fig 2.

The water flow is measured by electromagnetic flow meters and water rotameters. The electromagnetic flowmeter is KROHNE - OPTIFLUX 2100 and measures water flow in the range of 0.6 - 40 m3/h with an accuracy of 0.5%. A rotameter is utilized to measure flows less than 0.6 m3/h. Vertex flow meter and air rotameter are used to measure the airflow. The KROHNE Vertex flowmeter model OPTISWIRL 4070C has an accuracy of 2% at the maximum flow rate. At flow rates below 6 m3/h, air rotameters are used, and for flows above this value, the Vertex flowmeter is used. Four air rotameters are connected in parallel to measure airflow less than 6 m3/h. The description of the measuring equipment is summarized in the Table 1.

Table 1 Description of the measuring equipment.

Name	Description	Manufacturer	Accuracy (%)
Electromagnetic flowmeter	Measures water flow in the range of 0.6 - 40 m^3/h	KROHNE-OPTIFLUX 2100	0.5
Water rotameter	Measure flow less than 0.6 m^3/h.	KROHNE-VA40	1
Vertex flow meter	Measure flow rates more than 6 m^3/h	KROHNE-OPTISWIRL 4070C	2
Air rotameter	Measure flow rates less than 6 m^3/h	KROHNE – VA40	1

3. Electrical Resistance Sensor

An electrical resistance sensor is designed and built to calculate the volume fraction. The sensor design is shown in Fig. 3. This sensor consists of 8 electrodes made of stainless steel installed in the inner wall of the tube. The dimensions of each electrode are shown in Fig. 4. The electrodes are located inside the tube.

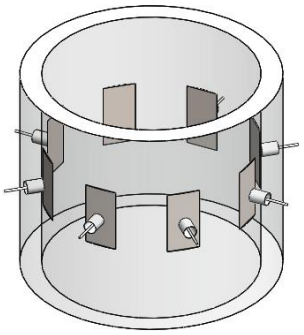

Fig. 3. Sensor design.

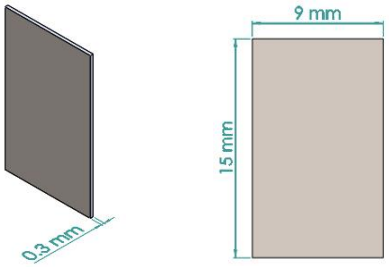

Fig. 4. Dimensions of electrical resistance sensor electrodes a) side view b) front view.

To minimize their disturbance on the flow, a thickness of 0.3 mm is considered for the electrodes. According to Fig. 5, in each step, an electric current is given to one electrode, and the electrical voltage is measured from the remaining seven electrodes. In the next step, the injection electrode (the electrode to which the electric current is applied) is changed and voltage is received from the other electrodes. The electrical current injection and voltage measurement process is performed for all eight electrodes, and voltage data are measured and recorded. The measurement time of each voltage data is 0.43 ms. Due to the similarity of some voltage data in each step, the number of recorded voltage data is reduced. In total 7 steps, 28 independent voltage data are measured and used to calculate the volume fraction. The measured voltage is related to phase distribution. So the bubbles' number or size variations cause changes in the measured voltage

Using voltage data measured by the electrical resistance sensor, the volume fraction can be obtained employing the Maxwell equation (Maxwell 1873).

$$\alpha_G = \frac{2\sigma_1 + \sigma_2 - 2\sigma_m - \sigma_m \frac{\sigma_2}{\sigma_1}}{2(\sigma_1 - \sigma_2) - \sigma_m \frac{\sigma_2}{\sigma_1} + \sigma_m} \quad (1)$$

where σ_m is the two-phase flow conductivity, $\sigma 1$ and σ_2 are the conductivity of the first phase(Water) and the second phase(Air), respectively. If the second phase is a nonconductor, the volume fraction can be calculated from Eq. (2).

$$\alpha_G = \frac{2\sigma_1 - 2\sigma_m}{2\sigma_1 + \sigma_m} \quad (2)$$

The conductivity of the first phase (σ_1) is obtained based on the electric current given to the electrodes in the electrical resistance sensor and the output voltage measured from the electrical resistance sensor when only a single phase of water is flowing in the testbed tube. The conductivity of two-phase flow (σ_m) is calculated by measuring the output voltage of the electrical resistance sensor when both air and water are flowing inside the testbed tube. Tocompare how the output voltage of an electrical

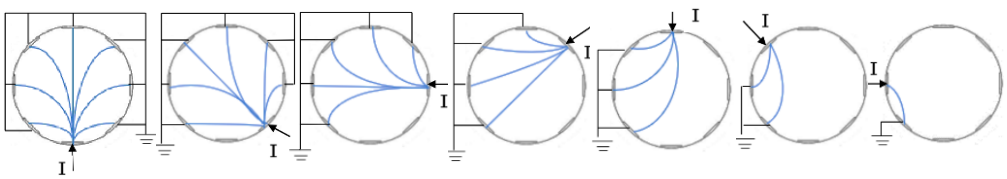

First step: 7 Data Second step: 6 Data Third step: 5 Data Fourth step: 4 Data Fifth step: 3 Data Sixth step: 2 Data Seventh step: 1 Data

Fig. 5. Method of injecting the electrical current into the electrodes.

resistance sensor changes with a volumetric fraction in a two-phase flow, the dimensionless number (v^*) is defined according to Eq. (3).

$$v^* = \frac{v_\circ - v_l}{v_l} \tag{3}$$

where v_o and v_l are the output voltage of the electrical resistance sensor for two-phase flow and single-phase water, respectively.

4. RESULTS AND DISCUSSION

4.1 Flow Pattern

By changing the superficial velocity of the fluids, three flow patterns are created as shown in Fig. 6. At a constant velocity of the liquid phase, the bubbly flow pattern is created at the low velocity of the gas phase. By increasing the gas phase's superficial velocity, the number and size of air bubbles increase. By increasing the coalescence between gas bubbles, the slug flow pattern is created. The slug flow pattern consists of large bubbles called the Taylor bubble, at the end of which is a series of tiny bubbles that follow the Taylor bubble. Further increase in gas phase velocity led to the breaking of Taylor bubbles and the transition of the slug flow pattern into the churn flow pattern.

4.2 Flow Pattern Map

To obtain a flow pattern map for a 50 mm diameter vertical pipe, flow patterns are generated and identified by changing the superficial velocity of the phases for 320 different phase states at the height of 270 cm from the testbed inlet. Bubbly, slug, and churn flow patterns are identified. The generated flow pattern map is drawn and compared with Taitel's flow pattern map (Taitel *et al.* 1980) as shown in Fig. 7.

It is observed that in the present study, compared to Taitel's flow pattern map, the slug flow pattern is

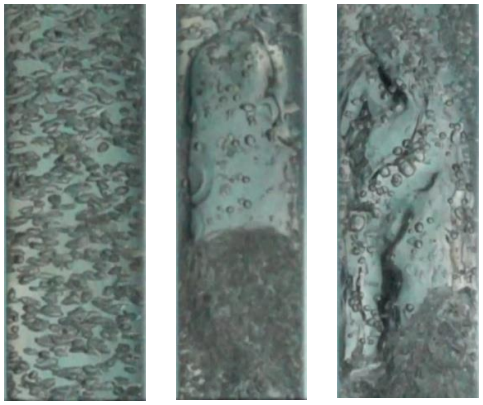

(a) (b) (c)

Fig. 6. Flow patterns in the tube with a diameter of 50 mm a) bubbly b) slug c) churn.

created at lower air velocities. The reason is the multi-stage air diffuser, which increases the number of gas bubbles. The more bubbles there are, the more likely the bubbles are to collide with each other. As the collision between bubbles increases, larger bubbles form, so the slug flow regime is formed sooner. In addition, the present study is an experimental study, while Taitel's flow pattern map is based on theoretical relationships in which the effect of fluids inlet geometry is not considered.

4.3 Volume Fraction

Dimensionless voltage variations are compared to the volume fraction obtained from the Maxwell equation for the slug flow pattern (Fig. 8). The variations are completely similar. The correlation of the dimensionless voltage changes with the volume fraction variations indicates that the volume fraction has a linear relationship with the voltage dimensionless number in the slug flow pattern. Therefore, the volume fraction is a coefficient of the dimensionless voltage.

9300 voltage data are measured for 4 seconds. The

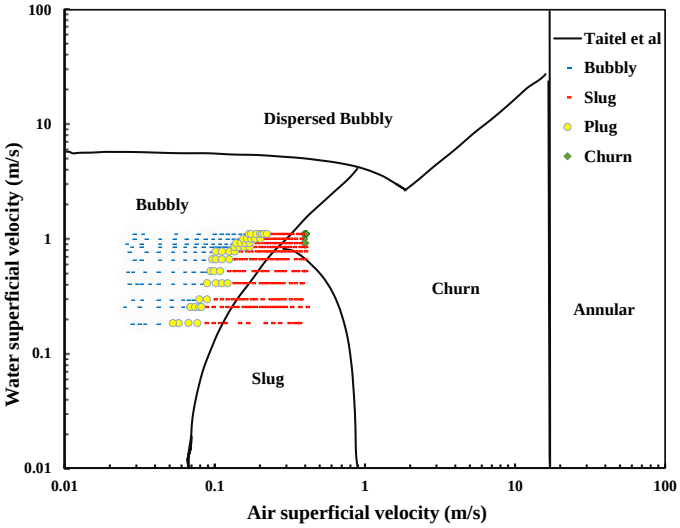

Fig. 7. Flow pattern map for pipe with the diameter of 50 mm at the height of 270 cm from the flow inlet.

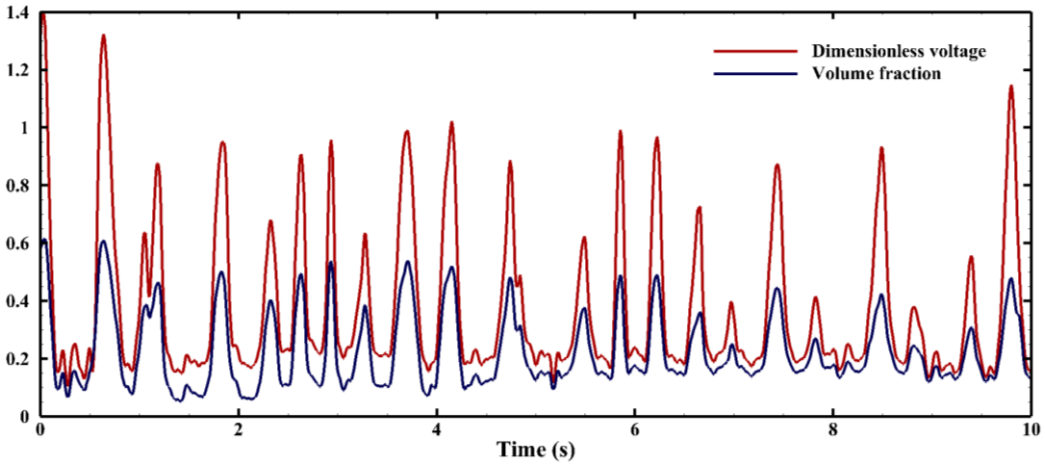

Fig. 8. Comparison of the volume fraction and the dimensionless voltage variations.

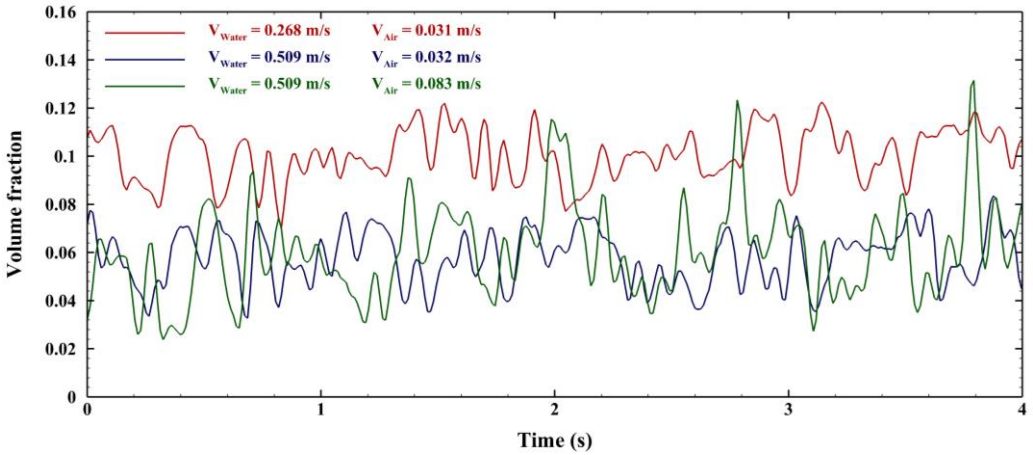

Fig. 9. Volume fraction changes in the bubbly flow pattern over time.

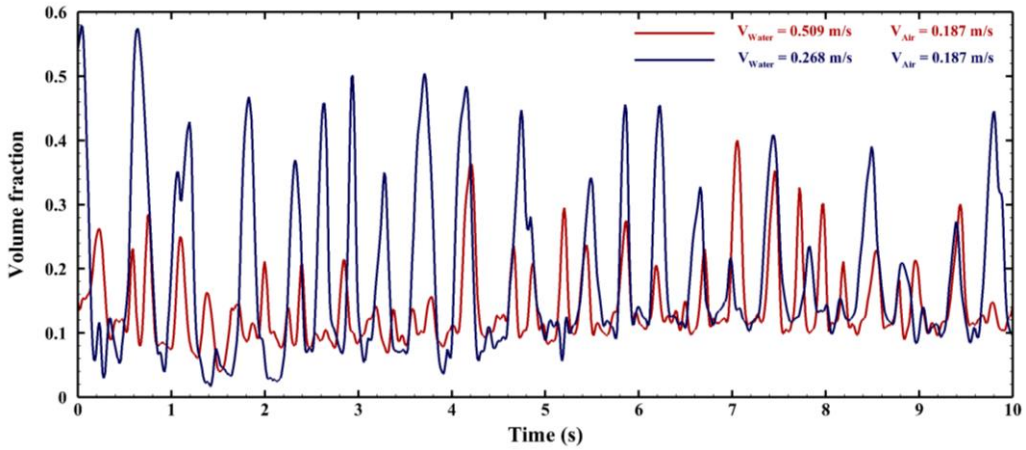

Fig. 10. Volume fraction changes in the slug flow pattern over time.

volume fraction value changes over time are plotted for the bubbly flow pattern at three different velocities of the phases. According to Fig. 9, by increasing the air superficial velocity at a constant water velocity, the volume fraction increases, and also by increasing the water superficial velocity at a constant air velocity, the volume fraction decreases. Volume fraction variations for slug flow pattern is plotted by measuring more than 23,000 voltage data in 10 seconds by the electrical resistance sensor (Fig. 10). The diagram shows that by increasing the water superficial velocity at a constant air velocity, the volume fraction decreases. As the water superficial velocity increases at a constant air velocity, the signal width decreases. The signal width is related to the length of the Taylor bubble in the slug flow pattern. The output signal width reduction due to the water velocity increase indicates that increasing the water velocity in a specified air velocity causes a slug flow with smaller Taylor bubbles. This is explained by the fact that by increasing the water velocity, the volume fraction of water in a certain volume of the

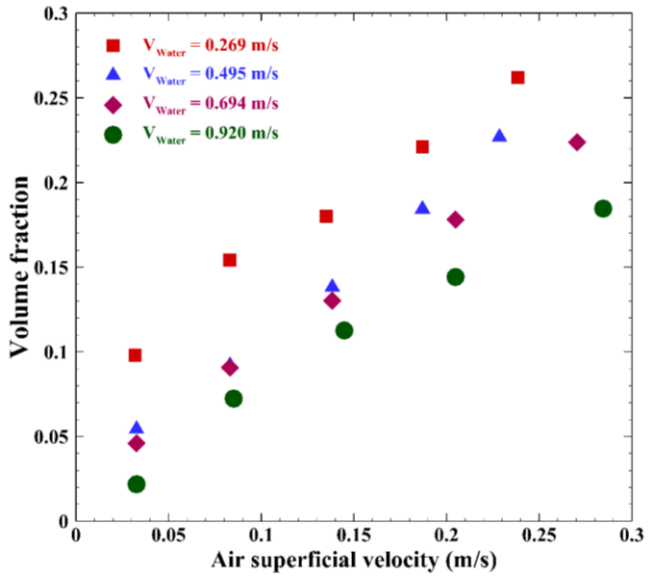

Fig. 11. Time-averaged volume fraction variations at different superficial velocities.

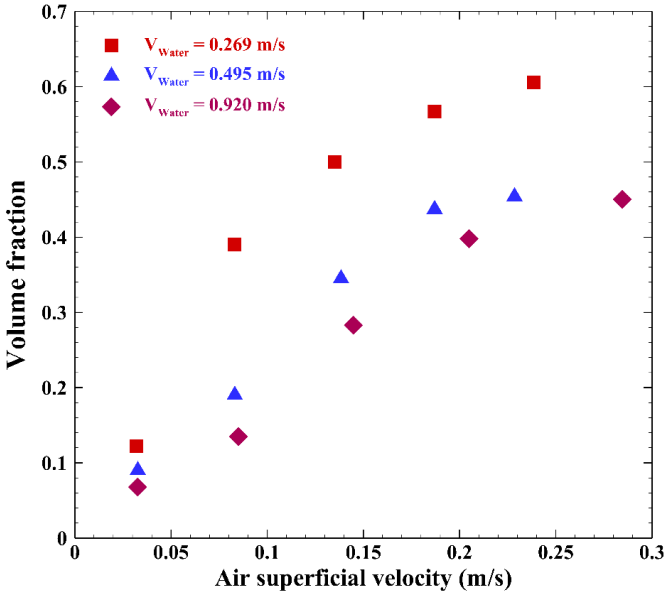

Fig. 12. Maximum volume fraction variations at different superficial velocities.

Table 2 Uncertainty in the volume fraction calculations.

Water superficial velocity (m/s)	Air superficial velocity (m/s)	Averaged volume fraction	Volume fraction uncertainty
0.694	0.033	0.045	0.492
0.694	0.083	0.091	0.017
0.694	0.138	0.124	0.503
0.694	0.205	0.170	0.525
0.694	0.270	0.224	0.156
0.920	0.033	0.022	0.024
0.920	0.085	0.082	0.568
0.920	0.014	0.111	0.512
0.920	0.205	0.155	0.702
0.920	0.285	0.186	0.773

pipe increases, and as a result, the amount of air in a certain volume decreases. As the air volume fraction decreases the air bubbles coalescence decreases. Increasing the water velocity also increases the velocity of the mixture flow, which causes the air bubbles to have less time to collide with each other, as well as to grow and enlarge.

The bubbly and the slug flow patterns are generated. Each of the generated patterns is sampled at each specified phase velocity for 8 seconds with the electrical resistance sensor. By using the measured data, the time-averaged volume fraction according to Fig. 11 is calculated and plotted for different phase velocities. By increasing the air superficial velocity at a constant water velocity, the time-averaged volume fraction increases. As the air inlet flow to the system increases, the amount of air inside the pipe

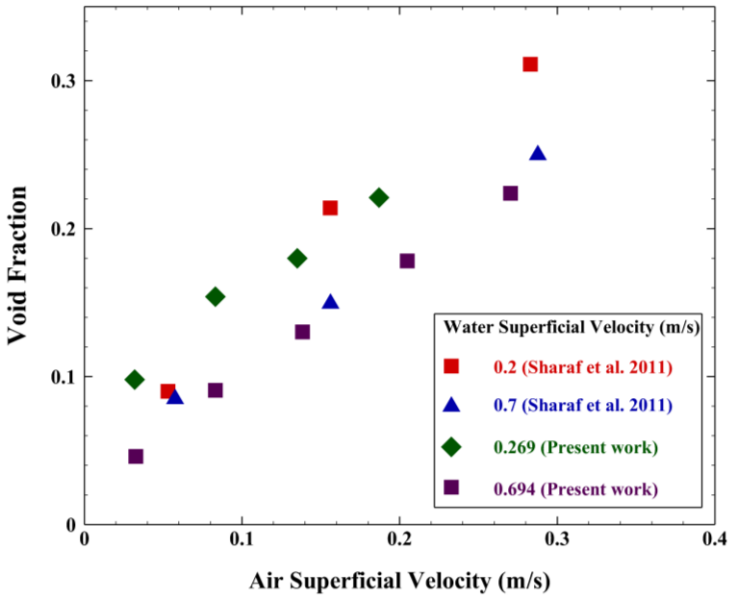

Fig. 13. Comparison of the present work with Sharaf *et al.* (2011)'s research.

increases, which leads to an increase in the volume fraction. Increasing the water velocity has the opposite effect on the volume fraction due to the increase in the water volume fraction. The variations of the maximum volume fraction during 8 seconds for the different velocities of each phase are shown in Fig. 12. As the gas phase velocity increases, the maximum volume fraction increases. In other words, as the gas phase velocity increases, the amount of air in a cross-section of the pipe increases, which indicates that the width or diameter of the Taylor bubble increases during the slug flow.

For several different velocities, the volume fraction variations are measured in three different time intervals. By averaging them, the uncertainty in measuring the volume fraction for each case is calculated and reported in Table 2. In Fig 13, for several different phase velocities, the volume fraction calculated in this study was compared with the volume fraction calculated by Sharaf *et al.* (2011), who used a gamma densitometry sensor. It can be seen that at almost the same speed of the phases, it has good matching results. The difference in the results can be due to the test conditions not being the same, including the type of inlet considered for the air inlet and the height of the installation of the sensors.

4.4 Comparison of High-Speed Camera Results with Electrical Resistance Sensor

Bubbly and slug flow patterns are recorded using a high-speed camera. By keeping the water superficial velocity constant and increasing the air superficial velocity, the flow pattern transition from bubbly to slug is evaluated by a high-speed camera. The evaluated results are compared with the volume fraction signal variations obtained from the electrical resistance sensor as shown in Fig. 14. It is observed that with increasing air velocity at constant water velocity, the number and concentration of bubbles in the images recorded by the high-speed camera increases, and the flow pattern changes from bubbly to slug. These changes in the number and type of bubbles indicate an increase in volume fraction with increasing air velocity.

The results obtained from the electrical resistance sensor are also presented along with the results of the high-speed camera. By placing the high-speed camera at the height of 270 cm from the flow inlet, the signal from the electrical resistance sensor is matched to the high-speed camera images to see the effect of the Taylor bubble length on the signal width. As shown in Fig. 15, at the constant velocity, as the length of the Taylor bubble increases, the signal width received from the sensor also increases. The relationship between the Taylor bubble length and the signal width at a specified phase velocity is almost linear.

The results demonstrate that at a constant water velocity, the length of the Taylor bubble increases with the air velocity increase in the slug flow pattern. Also, at a constant air velocity, the length of the Taylor bubble decreases as the water velocity increases, causing the output signal width of the electrical resistance sensor to decrease. The explanation for this is that by increasing the water velocity and consequently increasing the mixture velocity, smaller air bubbles are formed. Due to the high velocity of the flow, air bubbles have less opportunity to collide with each other and form larger bubbles. But at low water velocities, the bubbles move slower due to the lower flow rate. As a result, they have more time to collide with each other and form larger bubbles. Large bubbles has higher velocity than small bubbles. This issue causes large bubbles to collide with small bubbles, and makes the large bubbles larger.

According to Fig. 15, the phase velocity affects the length of the Taylor bubble as well as the signal width. An attempt is made to obtain a relationship between the signal width, the length of the Taylor

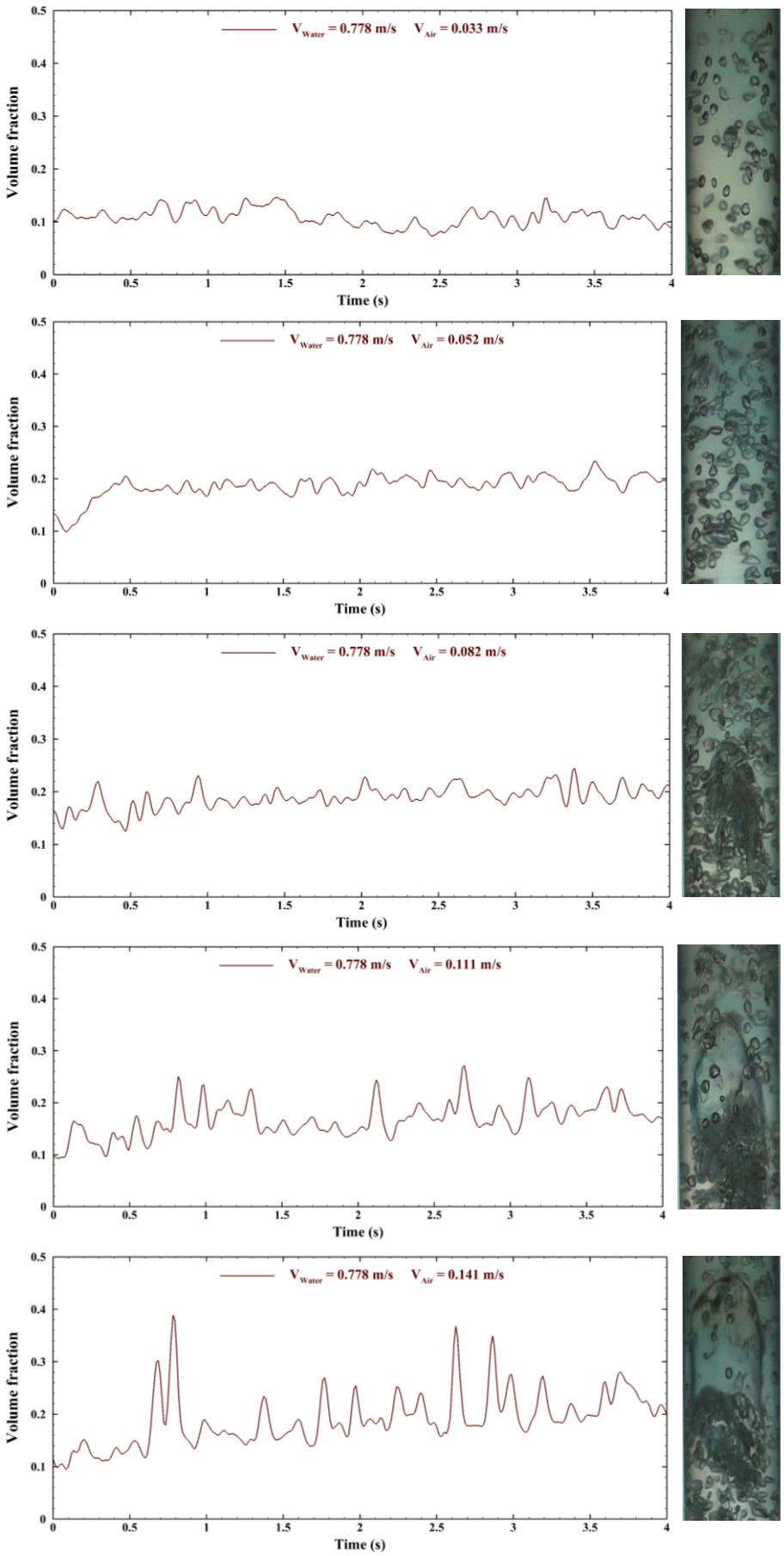

Fig. 14. Flow pattern and volume fraction variations by increasing the air velocity.

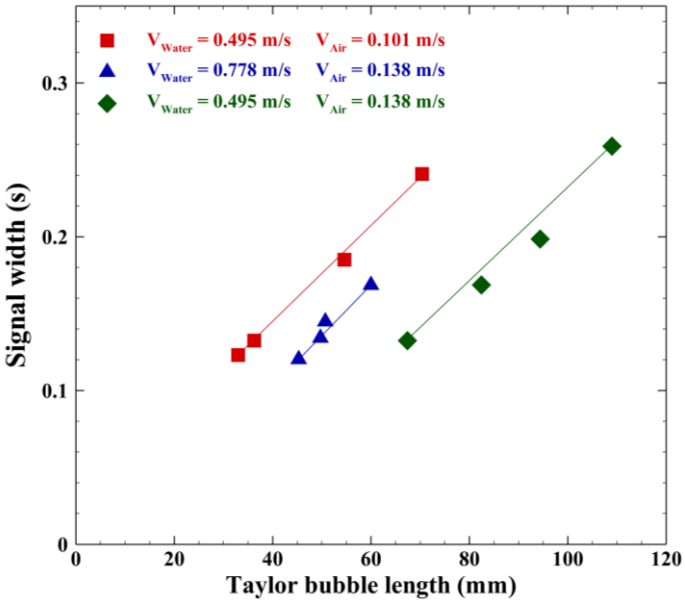

Fig. 15. Comparison of changes in signal Width of electrical resistance sensor with Taylor bubble length.

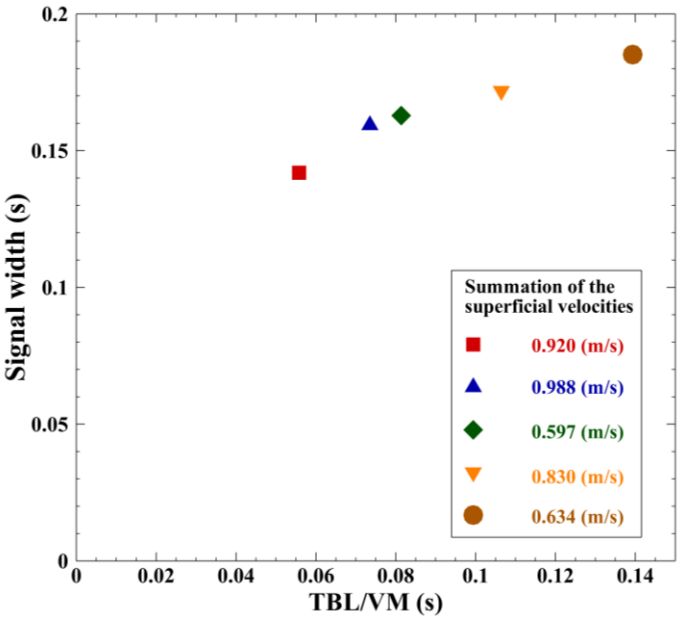

Fig. 16. Signal width changes with the ratio of Taylor bubble length to the total superficial velocity of the phases.

bubble, and the total superficial velocity of the phases. For each of the five different velocities of the phases, the mean signal width and mean Taylor bubble length is calculated using high-speed camera imaging. Imaging is done with a 960 fps camera for about 4 seconds.

The captured Taylor bubbles by the camera are evaluated using the image processing method, and the length of the bubbles is calculated. In order to calculate the length of the Taylor bubble, A ruler is placed next to the test bed tube and the flow pattern is filmed, By converting the video into a photo with the help of image processing software, the length of the Taylor bubbles that are available in the images can be obtained using a ruler scale.

Then, the obtained results are matched with the signals received from the electrical resistance sensor, and the signal width is calculated for each bubble. Figure 16 shows the variations of the mean signal width in terms of the ratio of the mean Taylor bubble length to the total superficial velocity of the phases. It is perceived that the changes are almost linear. By linear fitting of the data, a relationship in accordance with Eq. (4) is obtained to relate Taylor bubble length, signal width, and summation of the superficial velocities to each other. According to Eq. (4), by having the summation of the superficial velocities of the phases and the width of the signal, the length of the Taylor bubble can be predicted. By measuring a wider range of phase velocities, a more accurate and general relationship can be provided to

measure the length of the Taylor bubble. Because of the limitations in the imaging process of the Taylor Bubbles in one image frame (due to the large length of the Taylor bubble), it is not possible to capture the Taylor bubble in a wide range of superficial phase velocities. Therefore, more states are tested to obtain a more accurate relationship.

$$\text{signal width} = 0.4776\left(\frac{\text{Taylor bubble length}}{\text{summation of the superficial velocities}}\right) + 0.1206 \quad (4)$$

Since the pipes used in industry are generally metal, it is not possible to calculate the size of the Taylor bubble inside the pipe through observation and imaging. Therefore, the size of the created Taylor bubble inside the tube can be calculated by Eq. (4). The proposed equation can be used in the range of performed experiments in this study.

5. CONCLUSION

In the present study, an electrical resistance sensor was designed and built to calculate the volume fraction. The bubbly and the slug flow patterns were created and evaluated in a 50 mm diameter tube. By using the Maxwell relationship and the electrical resistance sensor, the temporal variations of volume fraction, the time-averaged volume fraction, and the maximum volume fraction for different phase velocities were calculated. The signal width and the Taylor bubble length variations for different phase velocities were investigated respectively by the electrical resistance sensor and the high-speed camera. An equation was presented to calculate the Taylor bubble length in terms of the electrical resistance signal width and the total superficial velocity of the phases. It was observed that with increasing air velocity at constant water velocity, the volume fraction and the number or size of air bubbles increase. The signal output from the electrical resistance sensor had an almost linear correlation with the Taylor bubble length. An accurate and comprehensive equation between the width of the signal output from the sensor and the length of the Taylor bubble makes the flow regime identification process easier. With the proposed equation, the length of the created Taylor bubble can be predicted based on the width of the output signal from the electrical resistance sensor without observing and imaging the flow.

REFERENCES

Bayle, J., P. Mege and T. Gauthier (2001). Dispersion of bubble flow properties in a turbulent FCC fluidized bed. *Fluidization X* 125-132.

Bennett, M. and R. A. Williams (2004). Monitoring the operation of an oil/water separator using impedance tomography. *Minerals Engineering* 17, 605-614.

Binns, R., A. R. Lyons, A. Peyton and W. Pritchard (2001). Imaging molten steel flow profiles. *Measurement Science and Technology* 12, 1132.

Brennen, C. E. (2005). *Fundamentals of Multiphase Flow*. Cambridge University Press.

Cui, H. and J. Chaouki (2004). Effects of temperature on local two-phase flow structure in bubbling and turbulent fluidized beds of FCC particles. *Chemical Engineering Science* 59, 3413-3422.

Das, R. and S. Pattanayak (1993). Electrical impedance method for flow regime identification in vertical upward gas-liquid two-phase flow. *Measurement Science and Technology* 4, 1457.

Dechsiri, C., E. Van der Zwan, H. Dehling and A. C. Hoffmann (2005). Dispersion of particle pulses in fluidized beds measured by positron emission tomography. *AIChE Journal* 51, 791-801.

Du, B., W. Warsito and L. S. Fan (2004). ECT studies of the choking phenomenon in a gas–solid circulating fluidized bed. *AIChE Journal* 50, 1386-1406.

Fan, L., T. C. Ho, S. Hiraoka and W. Walawender (1981). Pressure fluctuations in a fluidized bed. *AIChE Journal* 27, 388-396.

Fennell, P., J. F. Davidson, J. S. Dennis, L. F. Gladden, A. N. Hayhurst, M. D. Mantle, C. R. Müller, A. C. Rees, S. A. Scott and A. J. Sederman (2005). A study of the mixing of solids in gas-fluidized beds, using ultra-fast MRI. *Chemical Engineering Science* 60, 2085-2088.

Geldart, D. and J. Kelsey, (1972). The use of capacitance probes in gas fluidised beds. *Powder Technology* 6, 45-50.

Gilbertson, M., D. Cheesman and J. Yates (1998). Observations and measurements of isolated bubbles in a pressurized gas-fluidized bed. In *Fluidization IX*, Engineering Foundation Durango.

Halow, J. and P. Nicoletti (1992). Observations of fluidized bed coalescence using capacitance imaging. *Powder Technology* 69, 255-277.

Hänsch, S., D. Lucas, E. Krepper and T. Höhne (2012). A multi-field two-fluid concept for transitions between different scales of interfacial structures, *International Journal of Multiphase Flow* 47, 171-182.

Höhne, T. and C. Vallée (2010). Experiments and numerical simulations of horizontal two-phase flow regimes using an interfacial area density model. *The Journal of Computational Multiphase Flows* 2, 131-143.

Holland, D. J., Q. Marashdeh, C. Muller, F. Wang, J. S. Dennis, L. S. Fan and L. F. Gladden (2009). Comparison of ECVT and MR measurements of voidage in a gas-fluidized bed. *Industrial & Engineering Chemistry Research* 48, 172-181.

Hubers, J. L., A. C. Striegel, T. J. Heindel, J. N. Gray and T. C. Jensen (2005). X-ray computed tomography in large bubble columns. *Chemical Engineering Science* 60, 6124-6133.

Hulme, I. and A. Kantzas (2004). Determination of bubble diameter and axial velocity for a polyethylene fluidized bed using X-ray fluoroscopy. *Powder Technology* 147, 20-33.

Ishii, M. and G. De Jarlais (1986). Flow regime transition and interfacial characteristics of inverted annular flow. *Nuclear Engineering and Design* 95, 171-184.

Jia, J., H. Wang and D. Millington (2017). Electrical resistance tomography sensor for highly conductive oil-water two-phase flow measurement. *IEEE Sensors Journal* 17, 8224-8233.

Jin, H., S. Yang, M. Wang and R. Williams (2007). Measurement of gas holdup profiles in a gas liquid cocurrent bubble column using electrical resistance tomography. In *AIP Conference Proceedings*, American Institute of Physics.

Kaichiro, M. and M. Ishii (1984). Flow regime transition criteria for upward two-phase flow in vertical tubes. *International Journal of Heat and Mass Transfer* 27, 723-737.

Kotze, R., A. Adler, A. Sutherland and C. Deba (2019). Evaluation of electrical resistance tomography imaging algorithms to monitor settling slurry pipe flow. *Flow Measurement and Instrumentation* 68, 101572.

Kuidjo, K. and E. Vianney (2019). *Towards a Predictive Model to Reproduce Flow Regime Transitions in Gas-Liquid Flows with Neptune CFD: From a Dispersed to a Separated Regime*. Aix-Marseille.

Larachi, F. and J. Chaouki (2000). Non-invasive 3-D radioactive particle tracking in heterogeneous flows: principle & applications. *Recents Progres en Genie des Procedes* 14, 347-353.

Larachi, F., J. Chaouki, G. Kennedy and M. Dudukovic (1997). Radioactive particle tracking in multiphase reactors: principles and applications. In *Non-Invasive Monitoring of Multiphase Flows, Elsevier*.

Lirag Jr, R. C. and H. Littman (1971). *Statistical Study of the Pressure Fluctuations in a Fluidized Bed*. Rensselaer Polytechnic Inst., Troy, NY.

Marashdeh, Q., L. S. Fan, B. Du and W. Warsito (2008). Electrical capacitance tomography− a perspective. *Industrial & Engineering Chemistry Research* 47, 3708-3719.

Maxwell, J. C. (1873). *A Treatise on Electricity and Magnetism*. Clarendon press.

Meng, Z., Z. Huang, B. Wang, H. Ji, H. Li and Y. Yan (2010). Air–water two-phase flow measurement using a Venturi meter and an electrical resistance tomography sensor. *Flow Measurement and Instrumentation* 21, 268-276.

Montoya, G., E. Baglietto, D. Lucas, E. Krepper and T. Hoehne (2014). Comparative analysis of high void fraction regimes using an averaging euler-euler multi-fluid approach and a generalized two-phase flow (GENTOP) concept. In *International Conference on Nuclear Engineering*, American Society of Mechanical Engineers.

Noroozi, M. M., R. Maddahian, M. H. Ramezani and M. R. Ansari (2022). An LES-like multiscale multiphase flow model based on break-up and coalescence phenomena. *Journal of Applied Fluid Mechanics* 15(4), 1073-1085.

Patel, A. K., S. S. Waje, B. N. Thorat and A. S. Mujumdar (2008). Tomographic diagnosis of gas maldistribution in gas–solid fluidized beds. *Powder Technology* 185, 239-250.

Pedersen, S., C. Mai, L. Hansen, P. Durdevic and Z. Yang (2015). Online slug detection in multi-phase transportation pipelines using electrical tomography. *Ifac-Papersonline* 48, 159-164.

Peters, M. H., L. S. Fan and T. L. Sweeney (1983). Study of particle ejections in the freeboard region of a fluidized bed with an image carrying probe. *Chemical Engineering Science* 38(3), 481-485.

Ramezani, M., M. M. Noroozi, R. Madahian and M. R. A. Ansari (2021). Taylor bubble velocity measurement by using image processing. *Modares Mechanical Engineering* 21.

Rasteiro, M. G., R. C. Silva, F. A. Garcia and P. M. Faia (2011). Electrical tomography: A review of configurations and applications to particulate processes. *KONA Powder and Particle Journal* 29, 67-80.

Rehman, S. R., A. A. Zahid, A. Hasan, I. Hassan, M. A. Rahman and S. Rushd (2019). Experimental investigation of volume fraction in an annulus using electrical resistance tomography. *SPE Journal* 24, 1947-1956.

Schubert, M., G. Hessel, C. Zippe, R. Lange and U. Hampel (2008). Liquid flow texture analysis in trickle bed reactors using high-resolution gamma ray tomography. *Chemical Engineering Journal* 140, 332-340.

Shaikh, A. and M. H. Al-Dahhan (2007). A review on flow regime transition in bubble columns. International *Journal of Chemical Reactor Engineering* 5.

Sharaf, S., M. Da Silva, U. Hampel, C. Zippe, M. Beyer and B. Azzopardi (2011). Comparison between wire mesh sensor and gamma densitometry void measurements in two-phase flows. *Measurement Science and Technology* 22(10), 104019.

Sharma, A. K., K. Tuzla, J. Matsen and J. C. Chen (2000). Parametric effects of particle size and gas velocity on cluster characteristics in fast fluidized beds. *Powder Technology* 111, 114-

122.

Shi, T., C. Xie, S. Huang, R. A. Williams and M. Beck (1991). Capacitance-based instrumentation for multi-interface level measurement. *Measurement Science and Technology* 2, 923.

Sitnai, O. (1982). Utilization of the pressure differential records from gas fluidized beds with internals for bubble parameters determination. *Chemical Engineering Science* 37, 1059-1066.

Taitel, Y., D. Bornea and A. Dukler (1980). Modelling flow pattern transitions for steady upward gas‐liquid flow in vertical tubes. *AIChE Journal* 26, 345-354.

Tan, C. and F. Dong (2010). Cross correlation velocity of oil-water two-phase flow by a dual-plane electrical resistance tomography system. In 2010 *IEEE Instrumentation & Measurement Technology Conference Proceedings*, IEEE.

Vilar, G., R. Williams, M. Wang and R. Tweedie (2008). On line analysis of structure of dispersions in an oscillatory baffled reactor using electrical impedance tomography. *Chemical Engineering Journal* 141, 58-66.

Wahab, Y. A., R. A. Rahim, L. P. Ling, M. H. F. Rahiman, S. R. Aw, F. R. M. Yunus and H. A. Rahim (2018). Optimisation of electrode dimensions of ERT for non-invasive measurement applied for static liquid–gas regime identification. S*ensors and Actuators A: Physical* 270, 50-64.

Wang, F., Q. Marashdeh, L. S. Fan and R. A. Williams (2009). Electrical capacitance, electrical resistance, and positron emission tomography techniques and their applications in multi-phase flow systems. *Advances in Chemical Engineering* 37, 179-222.

Wang, F., Q. Marashdeh, L. S. Fan and W. Warsito (2010). Electrical capacitance volume tomography: Design and applications. *Sensors* 10, 1890-1917.

Wang, M., G. Lucas, Y. Dai, N. Panayotopoulos and R. A. Williams (2006). Visualization of bubbly velocity distribution in a swirling flow using electrical resistance tomography. *Particle & Particle Systems Characterization* 23, 321-329.

Wu, C., Y. Cheng, Y. Ding, F. Wei and Y. Jin. (2007). A novel X-ray computed tomography method for fast measurement of multiphase flow. *Chemical engineering science* 62, 4325-4335.

Xu, Y., H. Wang, Z. Cui and F. Dong (2009). Application of electrical resistance tomography for slug flow measurement in gas/liquid flow of horizontal pipe. In *2009 IEEE International Workshop on Imaging Systems and Techniques*, IEEE.

Xu, Z., Y. Jiang, B. Wang, H. Ji, Z. Huang and M. Soleimani (2020). Void fraction measurement of gas–liquid two-phase flow with a 12-electrode contactless resistivity array sensor under different excitation patterns. *Measurement Science and Technology* 31, 115103.

Yang, C., H. Wang and Z. Cui (2012). Application of electrical resistance tomography in bubble columns for volume fraction measurement. In *2012 IEEE International Instrumentation and Measurement Technology Conference Proceedings*, IEEE.

Yasui, G. and L. Johanson (1958). Characteristics of gas pockets in fluidized beds. *AIChE Journal* 4, 445-452.

Zhang, Y. and Y. Chen (2012). A novel PCA-SVM flow pattern identification algorithm for electrical resistance tomography system. In *Advances in Future Computer and Control Systems*, *Springer*.